



Broadband spectral characterization of the phase shift induced by population inversion in Ti:Sapphire

ROLAND S. NAGYMIHALY,^{1,2,5,*} HUABAO CAO,^{1,5} PETER JOJART,^{1,2} VIKTOR ZUBA,² ROLAND FLENDER,^{1,2} OLEG ANTIPOV,³ IMRE SERES,¹ ADAM BORZSONYI,^{1,2} VLADIMIR CHVYKOV,¹ KAROLY OSVAY,¹ AND MIKHAIL KALASHNIKOV^{1,4}

¹ELI-ALPS, ELI-HU Non-Profit Ltd., Dugonics tér 13 H-6720, Szeged, Hungary

²Department of Optics and Quantum Electronics, University of Szeged, P.O. Box 406 H-6701, Szeged, Hungary

³Institute of Applied Physics of Russian Academy of Science, 46 Ulyanov Street 603950, Nizhny Novgorod, Russia

⁴Max Born Institute for Nonlinear Optics and Short Pulse Spectroscopy, Max-Born-Strasse 2a 12489, Berlin, Germany

⁵These authors contributed equally to the paper

*roland.nagy Mihaly@eli-alps.hu

Abstract: The spectral phase shift of broadband amplified pulses, induced by population inversion, was measured in Ti:Sapphire at different pump fluence values. The measurement was performed for two orthogonal polarization directions and at two different crystal temperatures of 296 K and 30 K. Zero shifts and sign changes were observed in the spectral phase, which are connected to the gain spectrum of the crystal. The electronic refractive index changes were also numerically calculated by the Kramers-Kronig theory. The results are highly important for achieving sub-10 fs pulse duration and phase stability in the next generation of Ti:Sapphire-based laser systems.

© 2019 Optical Society of America under the terms of the [OSA Open Access Publishing Agreement](#)

1. Introduction

Ultrashort pulses with TW to multiple PW peak power are mostly generated by state-of-the-art Ti:Sapphire- (Ti:Sa) based chirped pulse amplification (CPA) systems [1,2]. The main reasons of using Ti:Sa crystals are the extremely large gain bandwidth and exceptional physical properties of the gain medium [3–5], the availability of the high energy pulsed pumping sources. Additionally, carrier-envelope phase (CEP) stabilization schemes can be easily implemented for Ti:Sa laser systems up to TW peak power [6,7]. Today the spectral bandwidth can be managed to obtain amplified pulses as short as 17 fs [8], or even 15 fs [9] after compression with multiple PW peak power. The increasing spectral bandwidth necessitates precise spectral phase control, which requires complete understanding of the dispersive effects occurring during the amplification process. It is well known, that in laser media as the pump radiation inverts the active ions, the refractive index of the medium can change. The inversion affects the spectral phase of amplified pulses, consequently shot-to-shot variations in the spectral phase can distort the temporal profile. This way the peak power of amplified pulses will be decreased, not to mention that the CEP stability can be also compromised.

Polarization-encoded CPA (PE-CPA) is a recently developed technique, which holds promise to support a gain bandwidth sufficient for compressed pulses in the few-cycle regime with Ti:Sa-based amplification [10–12]. Since this technique utilizes both gain cross-sections of the Ti:Sa crystal, the performance of this technique is affected by the phase fluctuations along the two axes. The gain cross section of Ti:Sa is significantly different for π - and σ -

polarized pulses, thus the spectral evolution of the refractive index change induced by inversion can be also different for the two polarizations.

Refractive index changes (RICs) due to population inversion are caused by the polarizability difference of the excited and unexcited rear-earth or transition-metal ions, and are known now for several laser crystals and glasses [13–15]. The RIC effect in Ti:Sa has been investigated before, however the effect was doubtfully stated to be insensitive to the signal wavelength [16]. For this reason, RICs induced by inversion need to be investigated in the gain band of Ti:Sa to establish the ultimate limitation of Ti:Sa amplification for reaching few-cycle pulses. Here, we have measured the wavelength dependent changes of refractive index caused by population inversion for both polarizations, which to the best of our knowledge, is the first spectrally resolved measurement of this effect in Ti:Sa.

2. Experimental technique

The effect of population inversion on the spectral phase shift was measured by using spectrally resolved interferometry (SRI) [17–19]. A single pass amplifier was realized in the sample arm of a Jamin interferometer (Fig. 1), where a cylindrical Ti:Sa crystal (8.45 mm thickness, 9 mm diameter, antireflection coated for 532 and 700–900 nm, absorption coefficient of 2.01 cm^{-1} at the pump wavelength) was placed in a cryogenic chamber. A conventional frequency-doubled Nd:YAG laser (Quanta-Ray, Spectra-Physics) with 7 ns, π -polarized pulses at 532 nm wavelength, running at 10 Hz repetition rate was used to excite the gain medium. The seed pulses are generated by a Ti:Sa-based CPA system at 200 Hz repetition rate and with a compressed pulse duration of 32 fs.

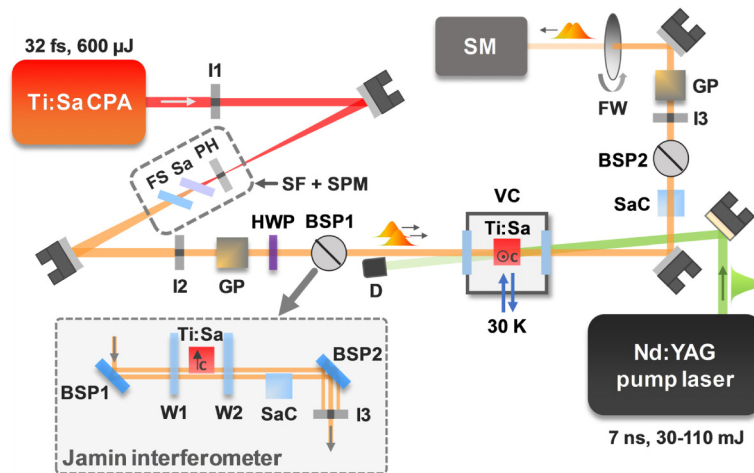


Fig. 1. Schematic layout of the experimental setup, highlighting the Jamin interferometer with more details in the bottom left inset. I1, I2 and I3 are irises, PH is a pinhole, Sa is a sapphire plate, FS is a fused silica plate, SF + SPM are spatial filtering and self-phase modulation, GP's are Glan polarizers, HWP is a broadband halfwave plate, BSP1 and BSP2 are beam splitter plates, D is a beam damper, VC is the vacuum chamber for cryogenic environment, SaC is a sapphire crystal, FW is reflective neutral density filter wheel, SM is spectrometer, while W1 and W2 are vacuum windows.

The required bandwidth was reached by spectral broadening of the compressed pulses via self-phase modulation (SPM). A combination of sapphire and fused silica (FS) plates with 1 mm thickness was used to obtain seed pulses covering the 700–900 nm wavelength range. A spatial filtering stage was inserted before the SPM, resulting in a smooth Gaussian beam profile. An aperture was used after the SPM to ensure that only the central part of the beam was selected (Fig. 1, I2 iris). For this reason, the change in the pulse spectrum was negligible across the beam profile.

The seed pulse with 70 μJ energy is split at the entrance of the interferometer by an uncoated FS plate in the vertical direction. The sample pulse with an $1/e^2$ diameter of 2 mm propagates through the pumped region of the Ti:Sa crystal, while the reference pulse is guided under the Ti:Sa medium, through a channel in the copper mount. An undoped, non-cooled sapphire crystal (SaC) with an identical thickness and optical axis orientation as the doped crystal was placed in the reference arm to compensate for dispersion. A few hundred fs group delay between the two arms was necessary to resolve spectral fringes in Fourier space, hence it is produced by the beam splitting stages and the slight difference between the Ti:Sa and sapphire crystals. After recombination with an identical FS plate and filtering out the additional reflections, the spectral interference of the sample and reference pulses is measured by a high-resolution spectrometer (Ocean Optics HR4000). The measurement of the spectral phase shift due to pump pulses was performed for both π - and σ -polarized pulses by tuning the polarization of the seed with a broadband halfwave plate before the interferometer. The pump energy fluence was tuned between 0.41 and 1.58 J/cm^2 with an $1/e^2$ spot size of 3 mm on the Ti:Sa crystal. This way the single pass gain for the π -polarized seed changed between 1.3 and 2.4, while the σ -polarization varied between 1.2 and 1.6. Room and cryogenic temperature conditions were investigated, where in the latter case the Ti:Sa crystal was cooled down to 30 K by a cryogenic refrigerator with liquid helium (CryoMech PT60). The interference fringes were recorded at 70 fps (Fig. 2), which ensured the detection of a portion of the 200 Hz pulse train as a background, and the pumped pulses at 10 Hz.

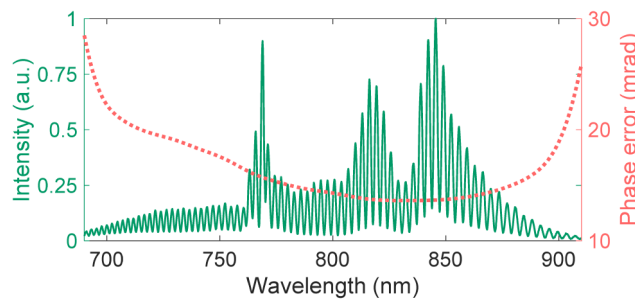


Fig. 2. Typical spectral interference fringe (green) and spectral phase error of a single measurement.

A typical measurement noise limit of sub-10 mrad standard deviation was reached for most of the phase spectrum (un-pumped pulses) due to the quasi-common-path layout of the interferometer. The typical phase noise increased to around 20 mrad in the case of pumping as a result of the energy stability (1.2% st. dev.) of the pump source (Fig. 2, red curve).

3. Room temperature phase shift

The phase shift induced by pump pulses was first measured at room temperature with the cryogenic refrigerator turned off. The copper mount and the metal housing of the refrigerator ensured enough heat extraction to keep the crystal temperature constant around 296 K for measurements with a duration of two minutes. At room temperature, the thermal phase shift has a decay on the millisecond time scale [20]. This was confirmed both by numerical modeling and measurements on our laser head for the temporally resolved temperature development, and a time window of 80 ms was calculated for the $1/e$ level of the peak temperature. On the other hand, the population inversion decays in 3.2 μs (room temperature lifetime of the excited energy level of Ti^{3+} ions). This way, the two different phase shift components can be de-coupled by changing the time delay of the pump pulse relative to the seed.

The starting time delay point was when the seed propagates through the crystal 50 ns after the pump pulse. Both the thermal and electronic phase shifts were measured at their maxima. However, when the time delay is increased to 10 μs , the population inversion drops to a negligible value, but the thermal inertia keeps the temperature-related phase shift practically at the same level as at the 50 ns delay. Decay of the inversion was measured by setting several time delays of the pump pulse up to 20 μs , and no change was found beyond 10 μs in the phase curve within the accuracy of the measurement. The total phase shifts were measured for both π - and σ -polarized pulses with 50 ns and 10 μs time delays relative to the pump pulse. The phase difference between the amplified and the previous unamplified pulses was calculated and averaged for 400 pulses. The phase difference measured at a 10 μs delay was subtracted from the 50 ns delayed one, giving the electronic phase shift only. Measurements were performed for different pump energy fluences, and thus for different gain values (Fig. 3). Phase curves measured for π -polarized pulses intersect collectively at zero shift, and a sign change was observed above 790 nm. The zero shift in the spectral phase is between 788 and 790 nm for the measured gain values, around the peak of the gain cross section line shape of Ti:Sa for π -polarized pulses at room temperature [20,21]. The phase shifts of σ -polarized pulses display similar convergence, but the intersection point is above 900 nm, outside of the spectral range of the interference pattern [Fig. 3(b)]. The deviation in the zero shift intersection is explained with the significant difference in the gain cross-section for the two differently polarized pulses. Further explanation will be given in Section 5.

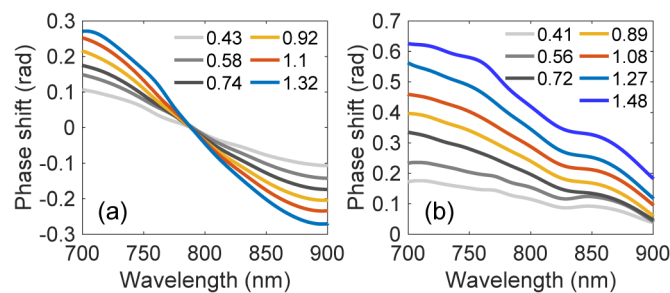


Fig. 3. Electronic phase shifts for different pump fluence values for π - (a) and σ -polarized (b) pulses at 296 K temperature. Color coding refers to the pump fluence in J/cm^2 .

The error in the determined phase shifts originated from the pump pulse energy fluctuation, which resulted in an averaged phase noise standard deviation of around 10 mrad for the π -, and 17 mrad for the σ -polarized pulses. The error was found to be around 30 mrad at the 900 nm edge of the spectrum is due to the lower signal-to-noise ratio of the recorded interferograms.

4. Cryogenic temperature phase shift

The decay time of inversion increases to about 4 μs by decreasing the crystal temperature to the range of 30-70 K [3,4]. However, as a result of the enormously increased thermal conductivity of Ti:Sa in this regime, the thermal relaxation decreases to around 10 μs , depending on the crystal sample and the coolant temperature. For this reason, the thermal and electronic phase shifts cannot be separated at 30 K the same way as in case of the room temperature scenario. To obtain the electronic phase shift, the phase shift induced by pumping was measured initially at the optimal 50 ns time delay between the seed and pump pulses. The thermal originated shift then had to be determined, and then subtracted from the measured spectral phase difference. For this reason, numerical simulations were conducted by using finite element method (COMSOL Multiphysics) on the different pump conditions. The geometry of our model only considered the Ti:Sa crystal. The heat dissipation rate accounts for 33.5% of the absorbed pump energy, since the quantum efficiency of Ti:Sa at this

temperature is close to unity [3,4]. All material properties were considered to be temperature dependent, and thermal conductivity of the sapphire host was taken from [5]. The simulations were performed in 3D, with the pump spot position and spatial distribution in the Ti:Sa crystal matching the experimental arrangement.

A measurement was performed on the χ thermo-optic coefficient for both π - and σ -polarized pulses, which contains all thermal processes affecting the refractive index. The spectral phase shift was measured from the start of the cryogenic refrigerator, while the temperature of the crystal holder was monitored with a type-T thermocouple. The interferometric and the temperature measurements were synchronized with the command control software. The wavelength dependence of χ was investigated for the 700-900 nm spectral range. No significant dependence was found within the sensitivity of the measurement for temperatures below 40 K. The values for this spectral region showed variations in the 10^{-8} 1/K range. There was no significant difference found in the χ values between for the two polarizations over the 30 to 60 K temperature range. Based on the measured χ , the thermal phase shift was calculated for the different pump fluence values. The thermal phase shifts were subtracted from the measured spectral phase changes at cryogenic temperatures (Fig. 4).

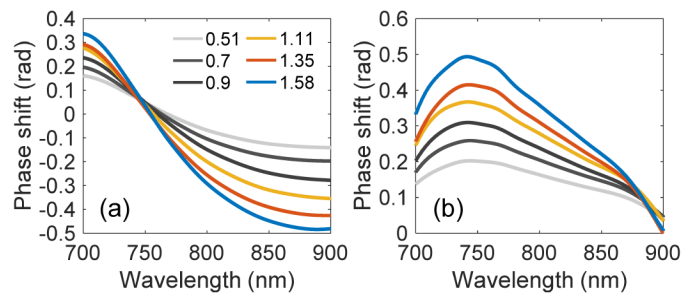


Fig. 4. Electronic phase shifts for different pump fluence values for π - (a) and σ -polarized (b) pulses at 30 K temperature. Color coding refers to the pump fluence in J/cm^2 , which is identical for the two polarizations.

At 30 K, the zero-phase crossing for π -polarized pulses is significantly blue-shifted to around 760 nm [Fig. 4(a)], and a zero-phase shift also appears for σ -polarized pulses around 900 nm. It is known that the gain spectrum of Ti:Sa is significantly blue-shifted to 765 nm at 77 K [21], which is expected to continue for lower temperatures. Shifting of the zero-phase crossing can be explained by this change in the gain spectrum at low temperature. On the other hand, the changes in the UV absorption spectrum of Ti:Sa due to the low temperature can have an effect on the zero-phase shift position. Deviation of the zero-phase intersection for π -polarized pulses at 30 K temperature spreads into the spectral range of 754 to 768 nm depending on the gain. This effect can be explained by the significant change of the gain cross-section due to the low temperature. The measured phase shifts had a noise of around 23 mrad for the π -, and 21 mrad standard deviation for the σ -polarized pulses. The observed phase error was higher at the 700 nm edge of the spectrum and found to be in the range of 35 mrad.

5. Refractive index changes

The effective RIC induced by inversion was calculated from the measured phase shifts with the total crystal thickness. Based on the inverted population density for the absorbed pump fluence, linear fitting was performed on the refractive index curves at different wavelengths (Fig. 5). The slope of the obtained linear fitting, i.e. the spectrally dependent RIC coefficient C_{inv} (derived by $C_{inv} = \delta n_e / \delta N_{up}$, where δN_{up} is the population change of the upper laser electronic level 2E) was visualized along the different wavelengths in Fig. 6. Based on the C_{inv}

coefficients, the δn_e RICs can be calculated at arbitrary inversion densities in the 700-900 nm wavelength range. The electronic RIC in Ti:Sa is caused by the ΔP polarizability difference of the excited and unexcited Ti^{3+} ions, where ΔP is the sum of all possible transition lines from the ground and excited states [22,23]. With the population of only one upper level, the differences in polarizabilities $\Delta P_{\pi,\sigma}$ are proportional to the RIC coefficients as

$$C_{\pi,\sigma} = \frac{2\pi F_L^2}{n_0^{\pi,\sigma}} \Delta P_{\pi,\sigma}, \quad (1)$$

where $F_L = \left[\left(n_0^{\pi,\sigma} \right)^2 + 2 \right] / 3$ is the local-field Lorentz factor, and $n_0^{\pi,\sigma}$ are the refractive indexes for the π and σ -polarized waves.

Within the gain line at 700-1000 nm the “resonant” contribution in ΔP , which is caused by the stimulated emission transition, can compensate for the “non-resonant” one originated by UV and visible absorption transitions (from ground and excited states of Ti^{3+} -ions), resulting in a zero-crossing and a sign change in ΔP . The emission cross-section for π -polarized pulses at 790 nm is almost three times higher than for σ -polarized pulses, results in the resonant contribution in ΔP for the π -transition being much stronger than that for the σ -transition.

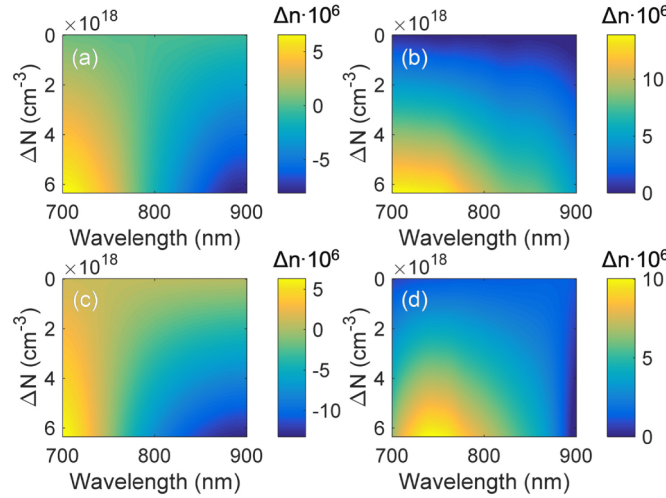


Fig. 5. Electronic RIC in the function of the inverted population density for π - (a,c) and σ -polarized (b,d) pulses at room and 30 K temperatures, respectively. The inversion density range corresponds to absorbed pump fluence values from 0 to 2 J/cm².

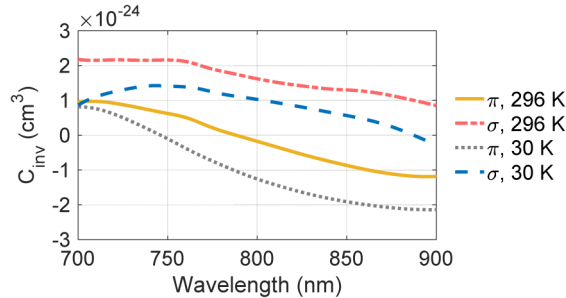


Fig. 6. Slope of linear fit to the RICs along the inverted population density in the investigated spectral range, for different polarizations and temperatures.

Based on the Kramers-Kronig relations [23–25], the δn_e electronic RIC induced by the δN_{up} population change of the upper laser level of a homogeneously-broadened active medium can be estimated at a given λ wavelength by

$$\delta n_e^{\pi,\sigma}(\lambda) = \frac{\delta N_{up}}{2\pi^2} P \int_0^\infty \frac{\Delta \sigma_m^{\pi,\sigma}(\lambda')}{(\lambda'^2 / \lambda^2) - 1} d\lambda', \quad (2)$$

where P refers to the Cauchy integral, and

$$\Delta \sigma_m^{\pi,\sigma}(\lambda) = \sigma_{ab}^{gr,\pi,\sigma}(\lambda) + \sigma_{em}^{\pi,\sigma}(\lambda) - \sigma_{ab}^{ESA,\pi,\sigma}(\lambda), \quad (3)$$

with $\sigma_{ab}^{gr,\pi,\sigma}$, $\sigma_{em}^{\pi,\sigma}$ and $\sigma_{ab}^{ESA,\pi,\sigma}$ being the cross-sections of the ground-state absorption, the emission and the excited-state absorption, respectively. In case of anisotropic crystals with lattice symmetries equal to or higher than orthorhombic (with collinear principal axes of the real and imaginary parts of the susceptibility), this estimation is valid for the main components [26]. Since the Ti:Sa crystal has a hexagonal symmetry of the lattice, the Kramers-Kronig relations are applicable for the π - and σ -components.

The Ti:Sa π - and σ -absorption cross-sections were determined by our direct absorption measurement at wavelength of 200-1000 nm. The cross-section differences of the emission and excited-state absorption in the 300-850 nm wavelength range were taken from [27], then an extrapolation to the wavelength ranges of 200-300 nm and 850-1300 nm was applied (Fig. 7). The numerical calculations of the RICs (for π - and σ -polarized transitions) normalized to population change of the upper laser level δN_{up} ($C_{\pi,\sigma}$ parameter) were performed by using Eq. (2). The sign changes were confirmed for both polarizations at room temperature (Fig. 8).

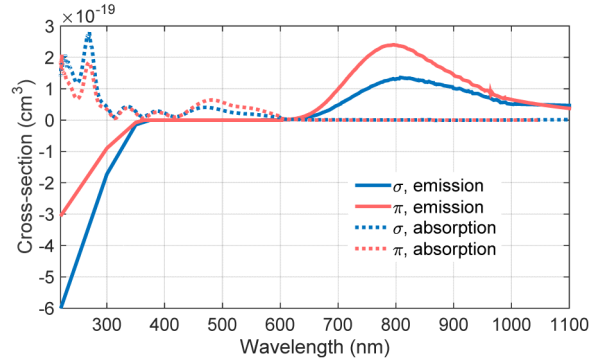


Fig. 7. The cross-sections for emissions $\sigma_{em}^{\pi,\sigma}$ minus the excited state absorption cross sections $\sigma_{ab}^{ESA,\pi,\sigma}$ (solid curves, blue for π -polarized transitions and red for σ -polarized transitions); and the cross-sections for the ground-state absorptions $\sigma_{ab}^{gr,\pi,\sigma}$ (dashed curves, blue for π -polarized transitions and red for σ -polarized transitions). These cross-sections were used for numerical calculations of the electronic RICs.

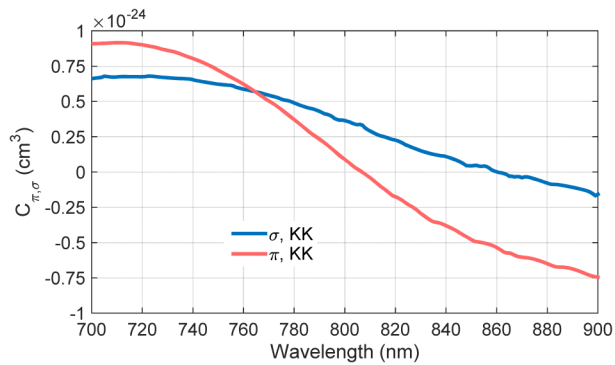


Fig. 8. The numerically calculated parameter $C_{\pi,\sigma}$ in the investigated spectral range for room temperature, where KK refers to the Kramers-Kronig theory.

According to Eqs. (1) and (2), the values of the $C_{\pi,\sigma}$ parameters were determined by the Kramers-Kronig integral depending on the emission, ground-state and excited state absorption cross-sections at UV, visible and near-IR wavelengths. In particular, this can explain the calculated difference of zero points of the inversion-induced RICs (where $C_{\pi,\sigma} = 0$).

The values of the numerically calculated C_{π} parameter agree well with the interferometrically measured C_{inv} coefficient for π -polarized pulses at room temperature (Figs. 6 and 8). On the other hand, the numerically calculated values of the C_{σ} parameter differ from the experimentally obtained results. This discrepancy can be explained by inaccurate determination of the ground-state and excited-state absorption in the UV wavelength range. The lack of measured data on the polarized absorption and emission spectra prevented us to perform the Kramers-Kronig calculation for the 30 K temperature case.

6. Conclusions and discussion

In conclusion, the population inversion induced RICs were investigated within the main emission band of Ti:Sa. By using the SRI method, spectral phase changes of amplified pulses were measured in a Jamin-type arrangement. The spectral phase shift induced by inversion for both π - and σ -polarized pulses was extracted at different pump fluence values. At room temperature, a zero-phase shift was found with a sign change at the peak of the gain spectrum, while for σ -polarized pulses no such behavior was observed in the investigated spectral range. By decreasing the temperature of the crystal to 30 K, similar behavior was found, however, the zero-phase crossing was found to be shifted to around 760 nm. The electronic RICs are explained by the polarizability difference between excited and unexcited Ti^{3+} ions in the crystal.

Based on the curves presented in Fig. 3 for the π -polarized pulses, i.e. for the case of conventional amplification in Ti:Sa, the effects on the temporal duration of amplified pulses were estimated for 100 TW to PW class systems. The population inversion in several amplifier stages with multiple passes leads to high order dispersion, which can be compensated by state-of-the-art AOPDF devices for every amplified pulse. Since the pulse energy fluctuation of high energy pump lasers for Ti:Sa systems can be as high as 5 to 8% peak to valley, the shot-to-shot changes of the pulse duration were also calculated. A worst-case scenario of ± 0.4 fs shot-to-shot variation of the compressed pulse duration was estimated for a conventional 1 PW amplifier system with five amplifier stages, in combination with a transform limited pulse duration of 15 fs, which is not critical. On the other hand, the shot-to-shot CEP noise can add up to a multiple radians through an amplifier chain due to the inverted Ti:Sa crystals. The currently known CEP stabilization feedback [6] or feed forward [28] loops seem not suitable in their current form to stabilize low repetition rate (10 Hz) PW-class amplifier systems [29]. For this reason, high energy stability (<0.5%

standard deviation) diode-pumped solid-state lasers are the best option as pumping sources to pave the way for CEP-stabilized high energy ultrashort pulses generated by Ti:Sa-based systems.

Beside the conventional CPA systems, the presented results are even more important in case of PE-CPA amplifiers. The efficiency of the polarization decoding after amplification in such arrangements strongly depends on the inversion induced phase shift for the two polarization directions. Additionally, because of the ultra-broadband amplified spectrum the phase shift difference between the two polarization directions has to be controlled for optimal compression. The pulse-to-pulse fluctuations are also more critical in the PE scheme, where CEP stability can gain higher importance as a result of the possibility of reaching few-cycle pulses.

Funding

ELI-ALPS (GINOP-2.3.6-15-2015-00001); Russian Academy of Science (Program I.7); Seventh Framework Programme (FP7, Laserlab Europe 654148); European Social Fund (EFOP-3.6.2-16-2017-00005).

References

1. Z. Gan, L. Yu, S. Li, C. Wang, X. Liang, Y. Liu, W. Li, Z. Guo, Z. Fan, X. Yuan, L. Xu, Z. Liu, Y. Xu, J. Lu, H. Lu, D. Yin, Y. Leng, R. Li, and Z. Xu, "200 J high efficiency Ti:sapphire chirped pulse amplifier pumped by temporal dual-pulse," *Opt. Express* **25**(5), 5169–5178 (2017).
2. A. Golinelli, X. Chen, E. Gontier, B. Bussi ere, O. Tcherbakoff, M. Natile, P. d'Oliveira, P.-M. Paul, and J.-F. Hergott, "Original Ti:Sa 10 kHz front-end design delivering 17 fs, 170 mrad CEP stabilized pulses up to 5 W," *Opt. Lett.* **42**(12), 2326–2329 (2017).
3. P. F. Moulton, "Spectroscopic and laser characteristics of Ti:Al₂O₃," *J. Opt. Soc. Am. B* **3**(1), 125–133 (1986).
4. P. Albers, E. Stark, and G. Huber, "Continuous-wave laser operation and quantum efficiency of titanium-doped sapphire," *J. Opt. Soc. Am. B* **3**(1), 134–139 (1986).
5. M. G. Holland, "Thermal conductivity of several optical maser materials," *J. Appl. Phys.* **33**(9), 2910–2911 (1962).
6. F. L ucking, V. Crozatier, N. Forget, A. Assion, and F. Krausz, "Approaching the limits of carrier-envelope phase stability in a millijoule-class amplifier," *Opt. Lett.* **39**(13), 3884–3887 (2014).
7. Y. Fu, E. J. Takahashi, and K. Midorikawa, "Indirect high-bandwidth stabilization of carrier-envelope phase of a high-energy, low-repetition-rate laser," *Opt. Express* **24**(12), 13276–13287 (2016).
8. S. K uhn, M. Dumergue, S. Kahaly, S. Mondal, M. F ule, T. Csizmadia, B. Farkas, B. Major, Z. V arallyay, E. Cormier, M. Kalashnikov, F. Calegari, M. Devetta, F. Frassetto, E. M ansson, L. Poletto, S. Stagira, C. Vozzi, M. Nisoli, P. Rudawski, S. Maclot, F. Campi, H. Wikmark, C. L. Arnold, C. M. Heyl, P. Johnsson, A. L'Huillier, R. Lopez-Martens, S. Haessler, M. Bocoum, F. Boehle, A. Vernier, G. Iaquaniello, E. Skantzakis, N. Papadakis, C. Kalpouzos, P. Tzallas, F. L epine, D. Charalambidis, K. Varj u, K. Osvay, and G. Sansone, "The ELI-ALPS facility: the next generation of attosecond sources," *J. Phys. B* **50**(13), 132002 (2017).
9. D. N. Papadopoulos, J. P. Zou, C. Le Blanc, G. Ch eriaux, P. Georges, F. Druon, G. Mennerat, P. Ramirez, L. Martin, A. Fr eneaux, A. Beluze, N. Lebas, P. Monot, F. Mathieu, and P. Audebert, "The Apollon 10 PW laser: experimental and theoretical investigation of the temporal characteristics," *High Power Laser Science and Engineering* **4**, e34 (2016).
10. M. Kalashnikov, H. Cao, K. Osvay, and V. Chvykov, "Polarization-encoded chirped pulse amplification in Ti:sapphire: a way toward few-cycle petawatt lasers," *Opt. Lett.* **41**(1), 25–28 (2016).
11. H. Cao, M. Kalashnikov, K. Osvay, N. Khodakovskiy, R. S. Nagymihaly, and V. Chvykov, "Active spectral shaping with polarization-encoded Ti:sapphire amplifiers for sub-20 fs multi-terrawatt systems," *Laser Phys. Lett.* **15**(4), 045003 (2018).
12. R. S. Nagymihaly, H. Cao, P. Jojart, M. Kalashnikov, A. Borzsonyi, V. Chvykov, R. Flender, M. Kovacs, and K. Osvay, "Carrier-envelope phase stability of a polarization-encoded chirped pulse Ti:Sapphire amplifier," *J. Opt. Soc. Am. B* **35**(4), A1–A5 (2018).
13. R. C. Powell, *Physics of Solid-State Laser Materials* (Springer-Verlag New York, 1998).
14. O. L. Antipov, A. S. Kuzhelev, A. Y. Luk'yanov, and A. P. Zinovev, "Changes in the refractive index of an Nd:YAG laser crystal on excitation of the Nd³⁺ ions," *Quantum Electron.* **28**(10), 867–874 (1998).
15. M. S. Kuznetsov, O. L. Antipov, A. A. Fotiadis, and P. M egret, "Electronic and thermal refractive index changes in ytterbium-doped fiber amplifiers," *Opt. Express* **21**(19), 22374–22388 (2013).
16. K. F. Wall, R. L. Aggarwal, M. D. Sciacca, H. J. Zeiger, R. E. Fahey, and A. J. Strauss, "Optically induced nonresonant changes in the refractive index of Ti:Al₂O₃," *Opt. Lett.* **14**(3), 180–182 (1989).
17. L. Lepetit, G. Cheriaux, and M. Joffre, "Linear techniques of phase measurement by femtosecond spectral interferometry for applications in spectroscopy," *J. Opt. Soc. Am. B* **12**(12), 2467–2474 (1995).

18. Dorrer and F. Salin, "Spectral resolution and sampling issues in Fourier-transform spectral interferometry," *J. Opt. Soc. Am. B* **15**(8), 2331–2337 (1998).
19. A. Borzsonyi, A. Kovacs, and K. Osvay, "What we can learn about ultrashort pulses by linear optical methods," *Appl. Sci. (Basel)* **3**(2), 515–544 (2013).
20. E. Byvik and A. M. Buoncristiani, "Analysis of vibronic transitions in titanium doped sapphire using the temperature of the fluorescence spectra," *IEEE J. of Quant. El.* **21**(10), 1619–1624 (1985).
21. H. Burton, C. Debardeleben, W. Amir, and T. A. Planchon, "Temperature dependence of Ti:Sapphire fluorescence spectra for the design of cryogenic cooled Ti:Sapphire CPA laser," *Opt. Express* **25**(6), 6954–6962 (2017).
22. O. L. Antipov, A. S. Kuzhelev, D. V. Chausov, and A. P. Zinoviev, "Dynamics of refractive-index changes in a Nd:YAG laser crystal under excitation of Nd³⁺ ions," *J. Opt. Soc. Am. B* **16**(7), 1072–1079 (1999).
23. R. Soulard, R. Moncorgé, A. Zinoviev, K. Petermann, O. Antipov, and A. Brignon, "Nonlinear spectroscopic properties of Yb³⁺-doped sesquioxides Lu₂O₃ and Sc₂O₃," *Opt. Express* **18**(11), 11173–11180 (2010).
24. J. Margerie, R. Moncorgé, and P. Nagtegaal, "Spectroscopic investigation of the variations in refractive index of a Nd:YAG laser crystal: experiments and crystal-field calculations," *Phys. Rev. B Condens. Matter Mater. Phys.* **74**(23), 235108 (2006).
25. V. Lucarini, J. J. Saarinen, K.-E. Peiponen, E. M. Vartiainen, *Kramers–Kronig Relations in Optical Materials Research* (Springer-Verlag Berlin Heidelberg, 2005).
26. M. Dressel, B. Gompf, D. Faltermeier, A. K. Tripathi, J. Pflaum, and M. Schubert, "Kramers-Kronig-consistent optical functions of anisotropic crystals: generalized spectroscopic ellipsometry on pentacene," *Opt. Express* **16**(24), 19770–19778 (2008).
27. T. Danger, K. Petermann, and G. Huber, "Polarized and time-resolved measurements of excited-state absorption and stimulated emission in Ti:YAIO₃ and Ti:Al₂O₃," *Appl. Phys., A Mater. Sci. Process.* **57**(4), 309–313 (1993).
28. S. Koke, C. Grebing, H. Frei, A. Anderson, A. Assion, and G. Steinmeyer, "Direct frequency comb synthesis with arbitrary offset and shot-noise-limited phase noise," *Nat. Photonics* **4**(7), 462–465 (2010).
29. F. Falcoz, "Towards high repetition rate ultra-intense lasers, latest developments at Amplitude Technologies," presented at the 8th Conference of the International Committee on Ultrahigh Intensity Lasers, Lindau, Germany, 9–14 Sept. 2018.